Cell, Vol. 117, 57–68, April 2, 2004, Copyright ©2004 by Cell Press

Conformational Antagonism between Opposing Active Sites in a Bifunctional RelA/SpoT Homolog Modulates (p)ppGpp Metabolism during the Stringent Response

Tanis Hogg,[1,2,6] Undine Mechold,[3,4,6,7] Horst Malke,[3,5] Mike Cashel,[4] and Rolf Hilgenfeld[1,2,*]

[1]Institute of Biochemistry
University of Lübeck
Ratzeburger Allee 160
D-23538 Lübeck
Germany

[2]Institute of Molecular Biotechnology
Beutenbergstr. 11
D-07745 Jena
Germany

[3]Institute for Molecular Biology
Jena University
Winzerlaer Str. 10
D-07745 Jena
Germany

[4]Laboratory of Molecular Genetics
National Institute of Child Health and Human Development
National Institutes of Health
Bethesda, Maryland 20892

[5]Department of Microbiology and Immunology
University of Oklahoma Health Sciences Center
Oklahoma City, Oklahoma 73190

Summary

Enzymes of the Rel/Spo family enable bacteria to survive prolonged periods of nutrient limitation by producing an intracellular signaling alarmone, (p)ppGpp, which triggers the so-called stringent response. Both the synthesis of (p)ppGpp from ATP and GDP(GTP), and its hydrolysis to GDP(GTP) and pyrophosphate, are catalyzed by Rel/Spo proteins. The 2.1 Å crystal structure of the bifunctional catalytic fragment of the Rel/Spo homolog from *Streptococcus dysgalactiae* subsp. *equisimilis*, Rel_{Seq}, reveals two conformations of the enzyme corresponding to known reciprocal activity states: (p)ppGpp-hydrolase-OFF/(p)ppGpp-synthetase-ON and hydrolase-ON/synthetase-OFF. The hydrolase and synthetase domains bear remarkable similarities to the catalytic domains of the cyclic phosphodiesterase and nucleotidyltransferase superfamilies, respectively. The active sites, separated by more than 30 Å, contain bound nucleotides including an unusual (p)ppGpp derivative, GDP-2′:3′-cyclic monophosphate. Reciprocal regulation of the antagonistic catalytic activities, suggested by the structure, is supported by mutagenesis experiments and appears to involve ligand-induced signal transmission between the two active sites.

*Correspondence: hilgenfeld@biochem.uni-luebeck.de
[6]These authors contributed equally to this work.
[7]Present address: Laboratoire "Oncogenese, Différenciation et Transduction du Signal," Institut André Lwoff, 7 rue Guy Moquet, 94800 Villejuif, France.

Introduction

In order to survive, bacteria must rapidly sense, and adapt to, continual changes in their environment. Complex strategies have evolved to allow rapid modulation of cellular functions when faced with diminishing nutrient supplies and other environmental pressures. Among these strategies is the stringent response, a pleiotropic physiological process involving alterations in metabolism and gene expression following the failure of aminoacyl-tRNA pools to keep up with the demands of protein biosynthesis. The abrupt global changes associated with the stringent response are triggered by the intracellular accumulation of derivatives of either GTP or GDP bearing a pyrophosphate group on the ribose 3′ hydroxyl position [guanosine 3′-diphosphate 5′-triphosphate or guanosine 3′,5′-bis(diphosphate)], collectively termed (p)ppGpp (for reviews, see Cashel et al., 1996; Chatterji and Ojha, 2001). Induction of (p)ppGpp synthesis is known to play multifarious roles in bacteria, such as quorum sensing in *Pseudomonas aeruginosa* (van Delden et al., 2001), antibiotic synthesis and differentiation in streptomycetes (Sun et al., 2001), bacteriocin production in *E. coli* (Kuhar et al., 2001), and virulence in *Legionella pneumophila* (Hammer et al., 2002) as well as *Mycobacterium tuberculosis* (Dahl et al., 2003). A (p)ppGpp-regulated stress-induced defense system analogous to the bacterial stringent response has also been found for plants (van der Biezen et al., 2000; Givens et al., 2004).

In *E. coli* and other proteobacteria, (p)ppGpp synthesis is driven by an 84 kDa ribosome-associated protein, RelA, which catalyzes a pyrophosphoryl group transfer of the β,γ-phosphates from ATP to the ribose 3′ OH of either GTP or GDP (E.C. 2.7.6.5). The (p)ppGpp-synthetase activity (hereafter simply referred to as "synthetase" activity) of RelA is stimulated by the stalling of ribosomal complexes on mRNA templates because of the nonenzymatic binding of cognate but deacylated tRNA in the aminoacyl-acceptor site. Degradation of (p)ppGpp is carried out in *E. coli* by SpoT, a 79 kDa cytosolic protein that, in a Mn^{2+}-dependent reaction, removes the 3′-diphosphate moiety to produce GTP (or GDP) and pyrophosphate [(p)ppGpp 3′-pyrophosphohydrolase activity (E.C. 3.1.7.2), henceforth abbreviated as "hydrolase" activity]. Despite extensive sequence homology between SpoT and RelA, RelA does not have hydrolase activity and SpoT displays only a weak synthetase activity (Mechold et al., 2002). Although the stringent response appears to be tightly regulated by two Rel/Spo enzymes in *E. coli*, bifunctional Rel/Spo homologs have been discovered in most gram-positive organisms studied, such as *Streptococcus dysgalactiae* subsp. *equisimilis* (henceforth designated *S. equisimilis*) (Mechold and Malke, 1997), *Bacillus spp*. (Wendrich et al., 2000), and *Mycobacterium tuberculosis* (Avarbock et al., 2000), implicating a single enzyme in the metabolism of (p)ppGpp (Mittenhuber, 2001). These bifunctional Rel/Spo enzymes appear to modulate (p)ppGpp levels through two distinct active sites that are controlled by

a reciprocal regulatory mechanism ensuring inverse coupling of opposing activities (Avarbock et al., 2000; Mechold et al., 2002). The demonstrated contribution of Rel/Spo homologs to virulence in pathogens such as *Legionella pneumophila*, *Mycobacterium tuberculosis*, and *Streptococcus pyogenes* (Hammer et al., 2002; Dahl et al., 2003; Steiner and Malke, 2000), together with the apparent absence of a mammalian Rel/Spo counterpart, make these enzymes viable targets for the design of antibacterial agents.

Here, we report the crystal structure of the catalytic N-terminal fragment (residues 1 to 385) of Rel_{Seq}, the bifunctional Rel/Spo homolog from *S. equisimilis*. Although the protein studied here lacks the C-terminal ribosome binding fragment, the structure of Rel_{Seq}1–385 fully explains the biochemical data available on both (p)ppGpp synthesis and hydrolysis. Two conformations are found that typify the opposing hydrolase-OFF/synthetase-ON and hydrolase-ON/synthetase-OFF states. The individual active sites conferring synthetase and hydrolase activities are located more than 30 Å from one another and have been identified within separate domains by structural and genetic analyses. An unusual cyclic guanosine nucleotide, ppG2′:3′p, has been identified in the hydrolase site of one of the two molecules in the crystallographic asymmetric unit, and appears to lock this entity in a hydrolase-ON/synthetase-OFF conformation. Conversely, the structure of the other molecule demonstrates that GDP binding to a catalytically competent synthetase site coincides with a nonproductive, unliganded state at the hydrolase center. A detailed picture emerges of the local and global conformational differences that correspond to the two states of reciprocal regulation of the opposing catalytic activities. All suggestions derived from the crystal structure are supported by mutagenesis or enzyme inhibition experiments. Structural kinships are found between the Rel/Spo hydrolase domain and the 3′,5′-cyclic-nucleotide phosphodiesterase superfamily (E.C. 3.1.4.17), as well as between the Rel/Spo synthetase domain and the nucleotidyltransferase superfamily (E.C. 2.7.7.-), particularly DNA polymerase β.

Results and Discussion

Overall Structure

The crystal structure of the bifunctional catalytic fragment of Rel_{Seq} (Rel_{Seq}1–385) was determined by a combination of multiwavelength anomalous dispersion (MAD) and multiple isomorphous replacement (MIR) (Tables 1 and 2). The crystallographic asymmetric unit contains two copies of Rel_{Seq}1–385 (Figure 1). Two catalytic domains are clearly evident within each monomer, with the hydrolase (residues 5–159) and the synthetase (residues 176–371) domains joined by an overlapping central 3-helix bundle (residues 135–195, denoted as C3HB throughout this paper).

Domain Topology

The N-terminal hydrolase domain is predominantly α-helical, with helices α1–α4 forming a 4-helix bundle. An extended loop (residues 39–51) forms a short β hairpin (β1–β2) between α2 and α3 and establishes part of the substrate binding pocket in the hydrolase active site (Figure 1). Helix α4 and the helical turn α5 are separated by His77 and Asp78 of the conserved "HD" motif found in the superfamily of metal-dependent phosphohydrolases (Aravind and Koonin, 1998). The C3HB consists of helices α8, α9′/α9″, and α10. Helices α9′ and α9″ nearly run along a common axis but are prevented from forming a continuous helix by a kink introduced by Pro173. Residues 5–197, including the hydrolase domain and the C3HB, represent a metal-dependent phosphohydrolase fold sharing substantial structural homology with the catalytic domain of cyclic nucleotide phosphodiesterases (PDEs) (Xu et al., 2000; Huai et al., 2003). PDEs are metallophosphohydrolases that also belong to the "HD-superfamily" (Aravind and Koonin, 1998) and regulate key cellular functions in higher organisms by catalyzing the degradation of intracellular nucleoside 3′,5′-cyclic phosphate second messengers (e.g., cAMP and cGMP) to their corresponding nucleoside 5′-phosphates. A superposition of the hydrolase domain of Rel_{Seq}1–385 and the catalytic domain of human PDE4 (Xu et al., 2000) gives a Cα root-mean-square deviation (r.m.s.d.) of 2.2 Å over a 110-residue core and reveals a common fold utilized by the Rel/Spo and PDE superfamilies for cleaving the nucleotide 3′-phosphoester bonds of their respective substrates—the key intracellular signaling molecules, (p)ppGpp and cNMP (Figures 2 and 3).

The C-terminal synthetase domain consists of a 5-stranded mixed β sheet (β3–β7) surrounded by five α helices (α11–α15) in a sandwich-like arrangement. Much of the polypeptide chain beyond residue 341 exhibits very poor electron density and appears to be

Table 1. Native Data: Collection and Refinement Statistics

Space group	C2
Unit-cell parameters (Å, °)	a = 173.5, b = 45.5, c = 126.5, β = 109.8
Wavelength (Å)	0.83
Resolution range (Å)	22.7–2.1
Number of reflections	195657
Number of unique reflections	53798
I/σ(I)	19.0 (2.1)
Completeness (%)	97.9 (96.5)
Multiplicity	3.6 (3.2)
R_{merge}[a] (%)	4.8 (37.7)
$R_{r.i.m.}$[b] (%)	5.6 (44.1)
$R_{p.i.m.}$[c] (%)	2.9 (23.0)
No. refined atoms	5426
R_{cryst}[d]	23.9 (30.5)
R_{free}[d]	27.3 (32.9)
rms deviations	
Bond lengths (Å)	0.015
Bond angles (°)	2.253

Values in parentheses refer to the highest resolution bin (2.15–2.10 Å).

[a] $R_{merge} = \Sigma_{hkl}\Sigma_i|I(hkl)_i - \langle I(hkl)\rangle|/\Sigma_{hkl}\Sigma_i I(hkl)_i$, where $I(hkl)$ is the intensity of reflection hkl and $\langle I(hkl)\rangle$ is the average intensity over all equivalent reflections.

[b] $R_{r.i.m.} = \Sigma_{hkl}(N/(N-1)^{1/2}\,\Sigma_i|I(hkl)_i - \langle I(hkl)\rangle|/\Sigma_{hkl}\Sigma_i I(hkl)_i$, where N is the multiplicity of the observed reflection (Weiss and Hilgenfeld, 1997).

[c] $R_{p.i.m.} = \Sigma_{hkl}(1/(N-1)^{1/2}\,\Sigma_i|I(hkl)_i - \langle I(hkl)\rangle|/\Sigma_{hkl}\Sigma_i I(hkl)_i$, where N is the multiplicity of the observed reflection (Weiss and Hilgenfeld, 1997)

[d] $R_{cryst} = \Sigma_{hkl}|F_o(hkl) - F_c(hkl)|/\Sigma_{hkl}F_o(hkl)$. R_{free} was calculated for a test set of reflections (5%) omitted from the refinement.

Table 2. Phasing Statistics

Data set[a]	Wavelength (Å)	Resolution (Å)	Completeness (%)[b]	Multiplicity	R_{merge}[c] (%)	R_{iso}[d] (%)	# Sites	
Phase Set 1: MAD phasing to 3.8 Å (mean FOM=0.72)								Diffraction ratios[e]
$HgCl_2$ λ1 (L-III inflection)	1.0083	3.8	96.0	8.2	5.2	-	-	0.033 (ano.)
$HgCl_2$ λ2 (L-I remote)	0.8266	3.8	97.5	7.3	5.2	-	4	0.047 (ano.)
λ2−λ1	-	-	-	-	-	-	-	0.052 (disp.)
Phase Set 2: MIR phasing to 3.0 Å (mean FOM=0.43)								Phasing power (cent./acent.)
Native	0.8445	3.0	96.1	3.6	4.3	-	-	-
$UO_2(NO_3)_2$	0.9102	3.5	79.8	4.2	9.7	31.3	5	0.67/0.77
K_2PtCl_4	0.9130	3.8	83.2	2.9	7.5	37.2	4	0.48/0.61
$HgCl_2$	0.8266	3.0	92.5	8.2	5.5	22.8	3	0.77/0.85
$UO_2(CH_3COO)_2$	1.0083	3.8	75.1	3.4	8.8	35.7	4	0.78/0.98
$KReO_4$	0.9102	3.5	77.3	3.5	15.5	26.6	1	0.51/0.51

[a] X-ray diffraction data measured at the following synchrotron beamlines: MAD dataset – ESRF beamline BM14 (Grenoble); Native – EMBL beamline BW7B (Hamburg); $UO_2(NO_3)_2$ and $KReO_4$ – EMBL beamline X11 (Hamburg); K_2PtCl_4 – Joint IMB-Jena/University of Hamburg/EMBL beamline X13 (Hamburg); $HgCl_2$ and $UO_2(CH_3COO)_2$ – ESRF beamline BM14 (Grenoble).

[b] Completeness is given for reflections where $F > 2\sigma$.

[c] $R_{merge} = \Sigma_{hkl}\Sigma_i|I(hkl)_i - \langle I(hkl)\rangle|/\Sigma_{hkl}\Sigma_i I(hkl)_i$, where $I(hkl)$ is the intensity of reflection hkl and $\langle I(hkl)\rangle$ is the average intensity over all equivalent reflections.

[d] $R_{iso} = \Sigma_{hkl}||F_{PH}(hkl)| - |F_P(hkl)||/\Sigma_{hkl}F_P(hkl)$, where $F_{PH}(hkl)$ and $F_P(hkl)$ are the derivative and native structure factor amplitudes, respectively.

[e] Observed diffraction ratios are measured as either the absolute value of the Bijvoet differences at a specific wavelength,

$$\left(\langle|F^+_{obs}| - |F^-_{obs}|\rangle^2\right)^{1/2} \Big/ \frac{1}{2}\left(\langle|F^+_{obs}|\rangle^2 + \langle|F^-_{obs}|\rangle^2\right)^{1/2},$$

or the dispersive differences between the two wavelengths,

$$\left(\langle|F^{\lambda 2}_{obs}| - F^{\lambda 1}_{obs}|\rangle^2\right)^{1/2} \Big/ \frac{1}{2}\left(\langle|F^{\lambda 1}_{obs}|\rangle^2 + \langle|F^{\lambda 2}_{obs}|\rangle^2\right)^{1/2}.$$

highly flexible, with the exception of the helical segment 363−371. The apparent flexibility of residues 342−362 is in agreement with high sequence variability within this region and a hypersensitivity to proteolytic cleavage (Mechold et al., 2002). The core of the synthetase domain exhibits the hallmark fold—a five-stranded mixed β sheet and two α helices—of the nucleotidyltransferase (NTase) superfamily (Holm and Sander, 1995). The closest known structural relative to the Rel/Spo synthetase domain is the palm domain of mammalian DNA polymerase β (pol β). Superposing the synthetase domain onto the palm domain of pol β in the (pol β)·(gapped DNA)·(ddCTP) complex (Sawaya et al., 1997) gives an overall Cα rmsd of 2.0 Å over a core of 67 equivalent residues (Figures 2 and 4), which is comparable to the fold similarity between individual NTases. Rel/Spo enzymes also contain an NTase-like catalytic motif within their synthetase domain (see below).

Nucleotide Binding to the Bifunctional Enzyme

We were surprised to discover that the two monomers in the asymmetric unit have dissimilar domain orientations, display different ligation states in the hydrolase domain, present different GDP binding modes in the synthetase domain, and exhibit topological heterogeneity around their corresponding active sites. For the sake of clarity, we have defined monomer 1 as the species having an unoccupied hydrolase site and a GDP bound synthetase site. Monomer 2 also contains a GDP molecule in its synthetase site, but the latter is in a catalytically incompetent conformation. In addition, monomer 2 exhibits electron density features within its hydrolase site that are consistent with the presence of an unusual GDP derivative, guanosine 5′-diphosphate-2′:3′-cyclic monophosphate (ppG2′:3′p) (Figure 3). The appearance of this nucleotide is confounding, as it was never utilized in our experiments.

The biological role of ppG2′:3′p remains largely unaddressed since it has never been directly identified as a stringent response metabolite. Another ppGpp derivative, i.e., ppGp (guanosine 5′-diphosphate-3′-monophosphate), has been implicated in the stringent response as a potent inhibitor of stable RNA synthesis (Pao et al., 1980). Further experiments showed that both ppGpp and ppGp effectively curtail purine biosynthesis by directly inhibiting IMP dehydrogenase and adenylosuccinate synthetase of the purine biosynthesis pathway, with ppGp being the stronger inhibitor (Pao and Dyess, 1981). More recently, a crystallographic study on adenylosuccinate synthetase reported that ppG2′:3′p, formed from ppGpp added to the crystals, was bound to the active site of the enzyme with an affinity at least two orders of magnitude greater than that of ppGpp, thus explaining enzyme inhibition by ppGpp (Hou et al., 1999). Our crystallographic evidence indicates this molecule may in fact exert inhibitory properties on the Rel/Spo protein itself, both as a competitive inhibitor of the hydrolase active site, and perhaps also in parallel (by virtue of inverse coupling of the opposing catalytic sites), as an "allosteric" inhibitor of synthetase activity (see below).

Neither the binding of GDP nor the recognition of ppG2′:3′p make use of the classical guanine nucleotide binding motifs (Bourne et al., 1990). Furthermore, there

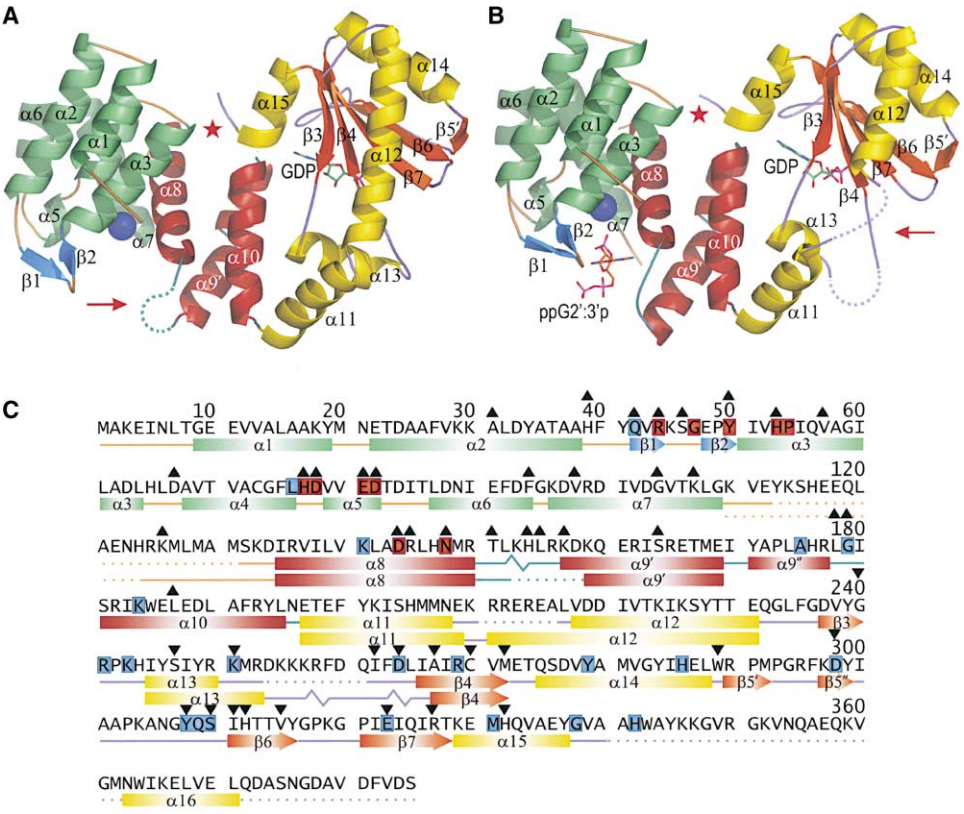

Figure 1. Structure and Sequence of Rel_{Seq}1–385

(A) Monomer 1 (hydrolase-OFF/synthetase-ON), in complex with Mn^{2+} (blue sphere) and GDP. Domain coloring: hydrolase, green α helices/blue β strands; synthetase, yellow α helices/orange β strands; central 3-helix bundle (C3HB), red. The disordered α8/α9′ loop is traced as a dashed line and highlighted by a red arrow. The small synthetase/hydrolase interdomain contact interface is labeled with a red star.

(B) Monomer 2 (hydrolase-ON/synthetase-OFF), in complex with Mn^{2+}, ppG2′:3′p and GDP. The disordered α11/α12 and α13/β4 regions are traced as dashed lines and highlighted with a red arrow.

(C) Primary and secondary structure of Rel_{Seq}1–385. Secondary structure for monomer 2 is shown beneath the sequence as bars (α helices), arrows (β strands), solid lines (loops and turns), jagged lines (3_{10}-helices), and dashed lines (disordered segments). Secondary structure is colored according to (A) and (B). Unique secondary structure assignments for monomer 1 are placed immediately below the corresponding assignment for monomer 2. Residues absolutely conserved throughout the mono- and bifunctional RelA and SpoT homologs are underlaid with blue boxes. Residues conserved in SpoT and the bifunctional enzymes but mutated in RelA homologs (hydrolase-incompetent) are marked with red boxes. Sites where missense point mutations lead to defective hydrolase and synthetase activities are indicated above the sequence line by upright and inverted black triangles, respectively (see text and Supplemental Data available on *Cell* website).

is no Walker-type motif (Walker et al., 1982) in Rel_{Seq} which might be involved in binding the phosphate groups of the pyrophosphate donor, ATP, yet the crystal structure suggests a highly charged phosphate binding site for this nucleotide (see below).

The (p)ppGpp 3′-Pyrophosphohydrolase Active Site

In monomer 2 of our structure, the guanine base of ppG2′:3′p fits into a deep cleft partially formed by residues 148−155 of the C3HB (including the C terminus of α8 and the subsequent α8/α9′ loop), as well as residues 44−46 of the β1/β2 loop (Figure 3). The base is sandwiched between the side chains of Lys45 and Leu155 on one side, and the side chains of Arg44 and Asn148 on the other, with the guanidinium group of Arg44 forming a π-stacking interaction with the guanine ring. In turn, the Arg44 side chain is held in place by direct H-bonds to the side chains of Asn148 and Thr151 as well as by a water-mediated H-bond to the hydroxyl of Ser46. Specific recognition of the guanine base is predominantly afforded by the β1/β2 and α8/α9′ loops, with H-bonding from the main-chain amides of Lys45 (to N-7 of ppG2′:3′p) and Ser46 (to O-6), and to the main-chain carbonyl of Thr151 (from N-1). An additional H-bond is made from N-2 of ppG2′:3′p to the main-chain carbonyl of Asn148 (α8). Arg44, Ser46, and Asn148 are all conserved in the metal-dependent phosphohydrolases of the Rel/Spo family, but notably mutated in the case of *E. coli* RelA and its hydrolase-incompetent homologs. Thr151 is occasionally replaced by Ser in the bifunctional Rel/Spo enzymes, emphasizing the importance of a γ-hydroxyl group for H-bonding with Arg44. This is underscored by our finding that the mutations T151P and T151A inactivate the hydrolase, as does R44Q. In fact, hydrolase-defective mutants were found for all residues numbered in Figure 3, except for Lys45 and Lys141 (see Supplemental Data, Supplemental Figure S1 available at http://www.cell.com/cgi/content/full/117/1/57/DC1).

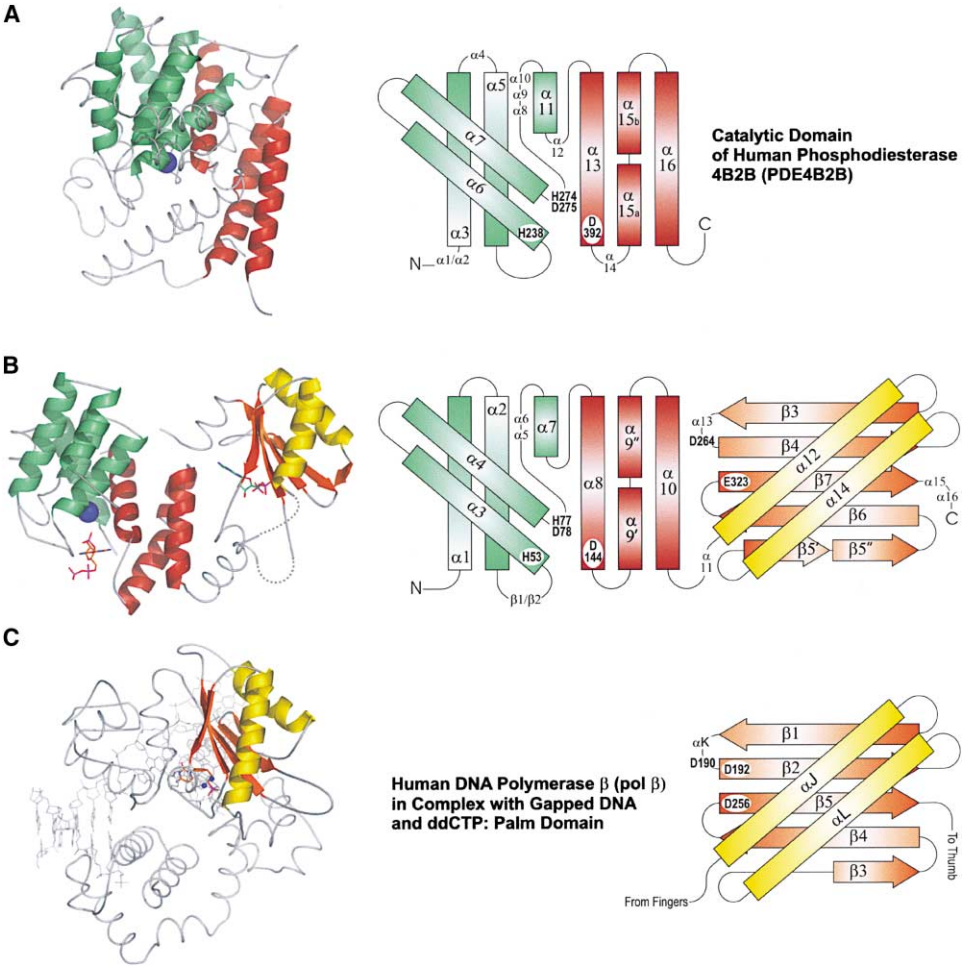

Figure 2. Similarities between the Catalytic Domains of Rel_{Seq}, Human Phosphodiesterase (PDE) and Human DNA Polymerase Beta (pol β)

Structural and topological diagrams highlighting equivalent folds and active-site residues for: (A) catalytic domain (residues 152−528) of PDE4; (B) Rel_{Seq}1–385; (C) catalytic domain (residues 10−335) of pol β. Homologous structural elements are displayed as ribbons; nonequivalent regions as thin gray lines. Monomer 2 of Rel_{Seq}1–385 is shown, with ppG2′:3′p, and GDP. Dark blue sphere, catalytic metal ion (Zn^{2+} for PDE4; Mn^{2+} for Rel_{Seq}). Conserved residues of the $H-X_{(n)}-HD-X_{(n)}-D$ metal binding tetrad are labeled in the accompanying topology diagrams (A and B). Two of the three catalytic carboxylates in pol β (Asp190 and Asp256, C) are also found in Rel_{Seq} (Asp264 and Glu323, B). Rel/Spo enzymes lack a counterpart for the second carboxylate of the D-X-D motif in NTases (Asp192 in pol β).

The 5′-diphosphate of ppG2′:3′p is widely exposed to bulk solvent and there is ample room for a γ-phosphate if present, i.e., in the case of pppGpp. The 2′:3′-cyclic phosphate moiety of ppG2′:3′p is projected into a pocket containing the essential Mn^{2+} cofactor. The Mn^{2+} is hexacoordinated in a distorted octahedral arrangement, with His53-Nε2 (α3), His77-Nε2 (C-cap of α4), as well as two water molecules filling the equatorial positions, and Asp78-Oδ2 (α4/α5 loop) and Asp144-Oδ1 (α8) occupying the apices (Figure 3). All residues are conserved in the bifunctional Rel/Spo enzymes and again mutated in *E. coli* RelA. The equivalent metal-coordinating residues in PDE4 (His238, His274, Asp275, and Asp392) are positioned in an identical manner (Figures 2 and 3), although the metal cofactors themselves appear to be different (Mn^{2+} in Rel/Spo; Zn^{2+} in PDE).

The mode of ppG2′:3′p binding in Rel_{Seq}1–385 provides an ideal template for modeling the natural substrate, (p)ppGpp, into the hydrolase pocket. On this basis, we propose that (p)ppGpp binding is characterized by coupling of the 3′ α- and β-phosphate groups to Mn^{2+} at the inner coordination-sphere positions occupied by the two water molecules in the ppG2′:3′p complex. In this configuration, two conserved carboxylate side chains, Glu81 and Asp82, would be located close to the 3′ α-phosphate of (p)ppGpp. Either of them could play a role by activating a water molecule for nucleophilic attack on the α-phosphorus atom. Indeed, we find mutant alleles of both residues (E81G and D82V) to inactivate the hydrolase (see Supplemental Figure S1 available on *Cell* website).

As evidenced in monomer 1, parts of loop α8/α9′ that are involved in forming one side of the guanine binding cleft unfurl and become disordered in the absence of ligand, specifically residues 153−155, along with the first turn of the α9′/α9″ helix (residues 156−158). Concomitant local displacements are observed in residues 40−50 including the β1/β2 hairpin. The most extensive main-chain atomic shifts in the hydrolase domain take place in residues 44−47 (Cα rmsd > 2.8 Å), culminating

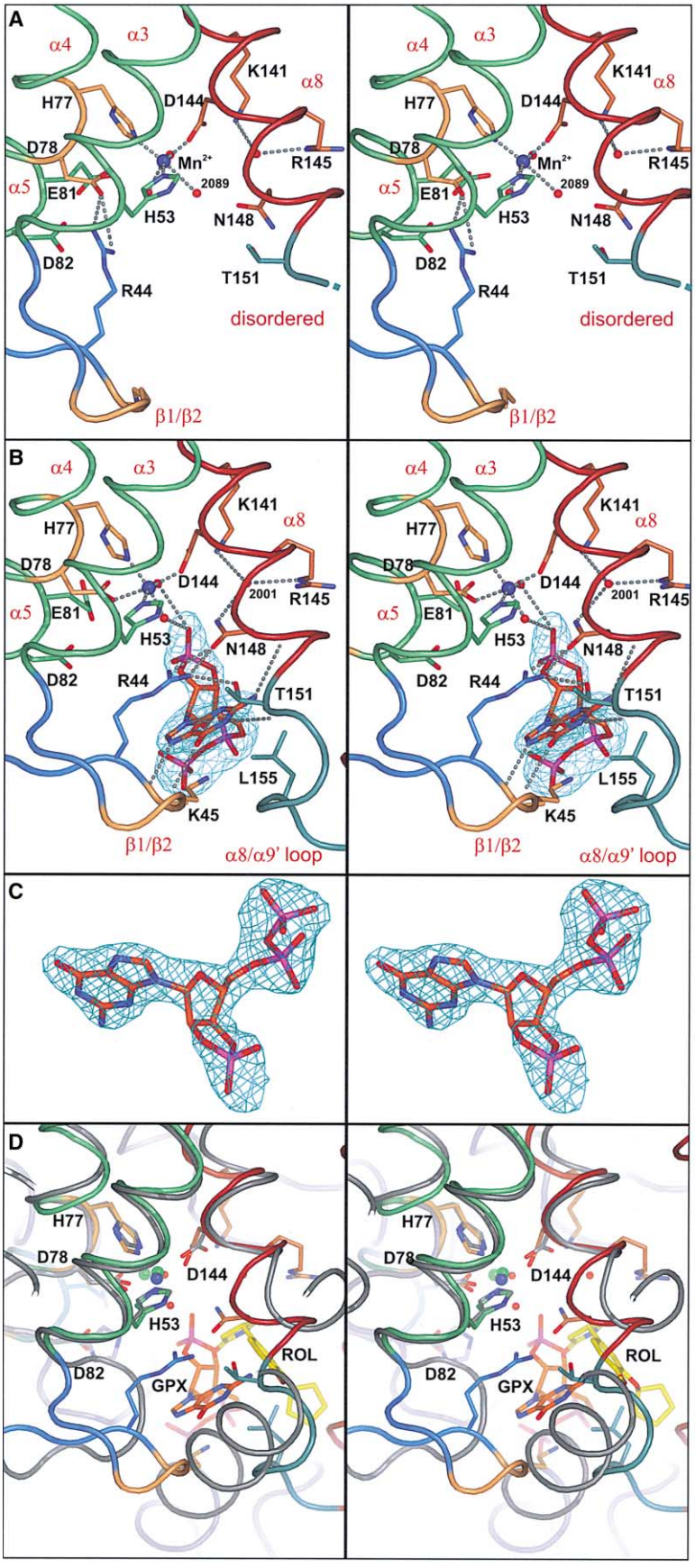

Figure 3. Conformations of the Hydrolase Site in Rel_{Seq}1–385 and a Superposition with PDE4

Active-site perspective and coloring are as in Figure 1. Secondary structure elements are identified with red labeling. Mn^{2+} (dark blue sphere), selected water molecules (red spheres), and H-bonds/Mn^{2+}-interactions (dashed lines) are illustrated.

(A) Stereo diagram depicting the hydrolase-OFF conformation (monomer 1). Mn^{2+} is pentacoordinated to His53, His77, Asp144, and two water molecules. An additional weak interaction (2.9 Å) takes place between the Mn^{2+} and wat 2089 (labeled).

(B) Stereo diagram showing the ligand bound, hydrolase-ON conformation (monomer 2). The 2mFo-DFc electron-density (blue mesh) for ppG2′:3′p is contoured at 1.5 σ. The Mn^{2+} is hexacoordinated, with Asp78 now participating in metal binding.

(C) Detailed stereo view of ppG2′:3′p in monomer 2 with corresponding 2mFo-DFc electron density contoured at 1.5 σ.

(D) Stereo superposition of Rel_{Seq}1–385 (monomer 2) and the PDE4-rolipram complex (Huai et al., 2003). PDE4 is rendered in gray shading. ppG2′:3′p (labeled "GPX") and (R)-rolipram (labeled "ROL") are respectively highlighted in orange and yellow. The two Zn^{2+} ions of PDE4 are visible as green spheres. The conserved metal binding H-$X_{(n)}$-HD-$X_{(n)}$-D tetrad (labeled according to Rel_{Seq} numbering) shows an identical positional arrangement in the two superfamilies, as does the core Mn^{2+}/Zn^{2+} ion.

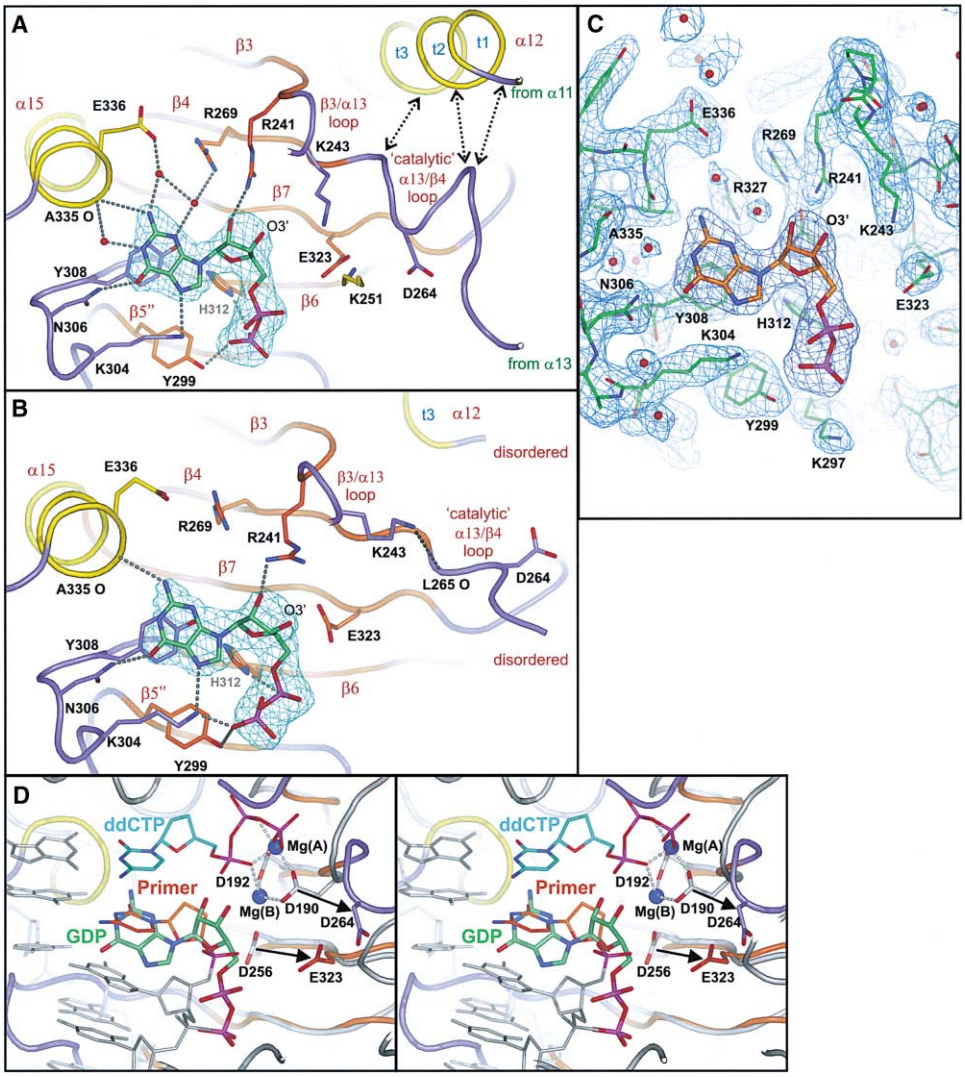

Figure 4. Conformations of the Synthetase Site in Rel_{Seq}1–385 and a Superposition with pol β

(A) The synthetase-ON conformation (monomer 1). Coloring is according to Figure 1; individual structural elements are labeled in red. The nucleophilic O3′ of GDP is marked. The final 2mFo-DFc electron density map, shown for GDP (blue mesh), is contoured at 1.0 σ. Selected H-bonds are shown as gray dashed lines. The catalytic loop (α13/β4) harboring Asp264 is stabilized in a 3_{10}-helical conformation through multiple van der Waals interactions (represented by black double-arrow dashed lines) with loop α11/α12 and the first two turns of α12 (labeled t1, t2). Chain traces extending from loops α11/α12, β3/α13, and α13/β4 are not visible due to image slab restrictions.

(B) The synthetase-OFF conformation (monomer 2). The α11/α12 loop and the first two turns of α12 are disordered; the resulting elimination of van der Waals contacts to the catalytic loop (α13/β4) leads to (1), partial refolding of the latter into an N-terminal extension of β4, and (2), disorder of residues 254–261 including the remaining residues of the catalytic loop and the C terminus of α13.

(C) Representative electron density in the synthetase site of monomer 1. GDP is highlighted in orange. The final 2mFo-DFc electron density map (1.0 σ) is overlaid as blue mesh.

(D) Stereographic superposition between the synthetase site of Rel_{Seq}1–385 (monomer 1) and the active site of pol β in the (pol β)·(gapped DNA)·(ddCTP) complex. The latter complex is rendered in gray shading with the exception of the primer 3′-terminal nucleotide (orange), ddCTP (cyan), and the two Mg^{2+} ions (dark blue). Rel_{Seq}1–385 and its GDP ligand are colored according to (A). The putative catalytic carboxylates of Rel_{Seq}, Asp264 and Glu323, are N terminally frameshifted by two residues relative to their pol β counterparts (indicated by black arrows).

in a dramatic side-chain rearrangement of Arg44: during its conformational transition from the ppG2′:3′p-bound to the ligand-free state, Arg44 loses its interdomain interactions with Asn148 and Thr151 of the C3HB and forms an intradomain salt-bridge with Asp78 (Figure 3). The newly established ion pair removes the carboxylate group of Asp78 from the inner Mn^{2+}-coordination sphere, thereby rendering a pentacoordinated Mn^{2+} species. This interdomain "clutch-and-release" mechanism of ligand binding and clearance is highlighted by considerable widening (>5 Å) of the (p)ppGpp binding cleft upon release of the ligand. The elegant rearrangements exhibited by Arg44 suggest it is not only central to the interdomain clutch-and-release mechanism of substrate binding but it also plays a critical role, along with Asp78 of the HD motif, in priming the Mn^{2+} for bidentate coordination to the 3′-diphosphate of (p)ppGpp. In agreement with this, the R44Q and D78A

mutations are found to abolish the hydrolase activity, whereas H77A retains significant activity; both types of modifications have only modest effects on the synthetase activity (Supplemental Figure S1 available on *Cell* website). The relative movements displayed by the hydrolase domain and C3HB upon ligand binding and release are part of a larger interdomain signal cascade that inversely couples the conformational states of the hydrolase and synthetase active sites (see below).

The (p)ppGpp-Synthetase Active Site

Both monomers present clear density for GDP in the synthetase site, which is located more than 30 Å away from the hydrolase site. As with the latter, the synthetase site comprises elements of the C3HB, albeit on the opposite side, with GDP fitting into a pocket partially formed by residues 176−185, including the C terminus of α9″, loop α9″/α10, and the N terminus of α10 (Figure 1). It is surprising that in spite of these interactions, we failed to identify a single random mutation in the C3HB that affected the synthetase while no less than 11 such mutations were found to diminish the hydrolysis reaction (see Supplemental Figure S1 available on *Cell* website). The guanine moiety of GDP stacks face-to-face against the phenolic ring of the strictly conserved Tyr308. Guanine-base recognition involves H-bonds from Lys304-Nζ to N-7, from N-2 to Ala335-O, and from Asn306-Nδ2 to O-6 (Figure 4).

We were intrigued to discover that the 3′-OH group of the GDP ribose moiety, which carries out the nucleophilic attack on the β-phosphorus atom of ATP during the synthetase reaction, does not make any H-bonds to the protein. This is of interest with respect to the identity of the residue, if any, that initiates the synthetase reaction by deprotonating the 3′-OH of GDP/GTP (Cashel et al., 1996). The remarkable structural homology between the synthetase domain of Rel_{Seq} and the palm domain of pol β led us to entertain the possibility that the respective active sites may contain similar catalytic groups. Indeed, the reactions catalyzed by Rel_{Seq} and pol β exhibit an element of mirror symmetry; the synthetase function of Rel_{Seq} catalyses a pyrophosphate transfer from ATP to the GDP/GTP 3′-OH with the release of AMP (GDP/GTP + ATP → (p)ppGpp + AMP), while the nucleotidyltransferase function of pol β carries out a dNMP transfer from dNTP to the primer 3′-OH with the release of pyrophosphate (primer + dNTP → primer-dNMP + PP_i). When we overlaid the activated synthetase domain of Rel_{Seq}1–385 with the palm domain of human pol β in the (pol β)·(gapped DNA)·(ddCTP) ternary complex (Sawaya et al., 1997), we found that the GDP molecule in the Rel_{Seq} synthetase site superimposes with the primer 3′-terminal nucleotide in the pol β complex. Furthermore, two of the conserved and catalytically essential carboxylic groups in the active site of pol β, Asp190 and Asp256, appear to correspond with the invariant Asp264 and Glu323 of Rel_{Seq} (Figures 2 and 4). Indeed, we find that Rel_{Seq} mutations D264G and E323Q eliminate detectable synthetase activity, without appreciably altering the hydrolase activity (see Supplemental Figure S1 available on *Cell* website). For all DNA polymerases, three conserved carboxylate residues have been implicated in the mechanism of nucleotidyl transfer, corresponding to Asp190, Asp192, and Asp256 of pol β. It has been shown from numerous crystallographic studies on pol β that these three aspartates are critically involved in the transferase mechanism by coordinating two essential Mg^{2+} cofactors, which in turn bind the deoxyribose 3′-OH of the primer strand and the phosphate groups of the incipient dNTP molecule. Because of its close proximity to the primer 3′-OH, Asp256 of pol β is also presumed to act as a general base in initiating the nucleophilic attack of the primer on the α-phosphorus of dNTP during polymerization. Based on the spatial and topological similarity between Glu323 in Rel_{Seq} and Asp256 in pol β, we propose an analogous function for the former in Rel_{Seq}, i.e., coordinating to Mg^{2+} and serving as the GTP/GDP 3′-OH proton acceptor during the (p)ppGpp-synthetase reaction. We should point out that the gap between Glu323-Oϵ1 and the 3′-OH of GDP is rather long at 6 Å, however it is likely that this distance will constrict substantially upon coordination of both groups to Mg^{2+}; such conformational rearrangements have been seen for Asp256 in pol β upon binding of the catalytic Mg^{2+} (Arndt et al., 2001).

In addition to GDP, we also added Mg^{2+} to our crystallization experiments but failed to localize the ion in our electron density maps, suggesting that the metal cofactor requires the presence of ATP (lacking in our crystallization buffer) to bind to the synthetase site with high affinity. Furthermore, the absence of a third conserved carboxylic residue in the synthetase active site (corresponding to Asp192 in pol β), implies that a second Mg^{2+} binding site is nonexistent in Rel/Spo enzymes. This structural observation supports existing biochemical evidence for a single-cation synthetase mechanism (Avarbock et al., 2000; Mechold et al., 2002), and strongly corroborates the notion that out of the eight known enzymes which catalyze a difficult nucleophilic substitution at the electron-rich β-phosphorus of NTP/dNTP substrates (Mildvan et al., 1999), members of the Rel/Spo family are exceptional in that they do not employ a dual divalent-cation mechanism. Adjacent to the GDP O3′ moiety and the putative single Mg^{2+} binding site, we find a cluster of several conserved basic side-chains (including Arg241, Lys243, and Lys251), which is likely involved in coordinating the β- and γ-phosphates of the pyrophosphate donor, ATP.

Based on our comparative analysis with pol β as well as the inactivating effect of the D264G allele, we can be reasonably certain that Asp264 is involved in binding the catalytic Mg^{2+} in the presence of ATP. Most strikingly, we detected pronounced conformational differences between the two monomers in the α13/β4 loop (containing Asp264), which we term the "catalytic loop." In monomer 1 (synthetase-ON), the carboxylate group of Asp264 is situated within the (p)ppGpp-synthetase active site ("IN" conformation) and is directed toward Glu323, with an intercarboxylate distance of 4.6 Å (ideally poised for Mg^{2+} coordination upon ATP binding). However, the active site configuration is drastically altered in monomer 2 (synthetase-OFF), where Asp264 is far removed from the synthetase pocket ("OUT" conformation) and the corresponding intercarboxylate distance stretches to ∼14 Å (Figure 4), indicating a nonproductive state for Mg^{2+}-ATP binding.

Reciprocal Regulation of Catalytic Activities

It is established that both the bifunctional Rel/Spo enzymes studied in some detail, Rel_{Seq} and Rel_{Mtb}, display an aversion to simultaneously activating synthetase and hydrolase (Avarbock et al., 2000; Mechold et al., 2002). This feature could be rationalized as avoiding futile cycling of synthesis and hydrolysis of (p)ppGpp at the expense of ATP, or as a way to facilitate rapid adjustments of (p)ppGpp levels. The C-terminal half of Rel_{Seq}, which binds to the ribosome and senses the presence of nonacylated tRNAs and which is not part of the protein structure reported here, is involved in reciprocal regulation of the two catalytic activities. Addition of this portion of Rel_{Seq} to the catalytic fragment leads to a 50-fold activation of the hydrolase and a simultaneous 25-fold reduction of the synthetase (Mechold et al., 2002). This suggests that intramolecular crosstalk between the opposing catalytic sites is an intrinsic property of the protein. The crosstalk can be interrupted by some of the mutations described above that selectively inactivate one but not the other of the two catalytic activities. On the other hand, the binding of nonreactive nucleotide analogs to one of the active sites should influence the opposing catalytic activity. We have found that addition of α,β-methylenyl ATP (AMPCPP), an analog incapable of pyrophosphate transfer by the synthetase in the presence of GTP, at concentrations equal to those of the substrate, ATP, not only led to severe inhibition of the synthesis of pppGpp (data not shown) but also to a reduction of the hydrolysis reaction by a factor of about four (Supplemental Figure S2 available on *Cell* website).

Only a small handful of enzymes are known to catalyze opposing reactions at distinct active sites. Some of these, such as 6-phosphofructo-2-kinase/fructose-2,6-bisphosphatase, employ a regulatory strategy involving covalent modification (Kitamura et al., 1988). However, enzymatic regulation by covalent modification requires a continuous and substantial expenditure of energy, and there exists selective pressure for energy-efficient control mechanisms (Goldbeter and Koshland, 1987). In this light, allosteric regulation may be viewed as cost-effective means for controlling enzymatic processes.

The two conformations of Rel_{Seq}1–385 detailed above, with monomers 1 and 2 respectively signifying the "hydrolase-OFF/synthetase-ON" and "hydrolase-ON/synthetase-OFF" states of the enzyme, seem to provide solid structural evidence for the mode of intramolecular signal transmission between the active sites. Figure 5 displays an atomic displacement profile between the monomers, showing how ligand binding to the hydrolase domain triggers a signal amplification cascade into the adjacent synthetase domain. Using our clutch-and-release analogy presented earlier, elevated levels of (p)ppGpp (represented by the derivative ppG2′:3′p in monomer 1) stimulate a clutching motion between the hydrolase domain and the C3HB to trap the nucleotide within the hydrolase active site. The initial rearrangement of the β-hairpin, $\beta1/\beta2$, which exhibits a translational amplitude of 2.8 Å at Lys45 and Ser46 at the tip of the turn (visible as a strong peak in Figure 5B), leads to disruption of the ion pair between Arg44 and Asp78. The latter joins the coordination sphere of the Mn^{2+} ion, thus activating the hydrolysis reaction. The rigid movement of the C3HB toward the hydrolase domain is actuated by a shift of $\alpha8$ residues Asn148 and Thr151 to establish H-bonds with the repositioned Arg44 and with the guanine base of ppG2′:3′p (Cα shift of 2.9 Å for Thr151). The rigid-body rearrangement of the C3HB can be observed as the second plateau (residues 135−195) of the signal cascade in Figure 5B.

Amplification of the signal manifests itself due to the inability of the synthetase domain to move in phase with the C3HB. This breakdown in tandem movement occurs because of a tight hydrophobic interface involving residues 337−340 of the synthetase domain (C-terminus of $\alpha15$ and succeeding loop), which are sandwiched between residues 64−66 (loop $\alpha3/\alpha4$) of the hydrolase domain and residues 178−180 (loop $\alpha9'/\alpha10$) of the C3HB. This interface imposes a local restraint on the movements of the synthetase domain (with residues 337−340 exhibiting the lowest rmsd within it; Figure 5B), which in turn affects its global motion: the bulk of the synthetase domain exhibits a lateral swinging movement with respect to the C3HB, hinged on two primary contact points with the latter (Figure 5). The first of these hinge points is established by the anchoring of the N terminus of $\alpha13$ (Ile245−Tyr246) into a V-shaped cleft formed by the diverging $\alpha10$ and $\alpha11$ (marked by a magenta dot in Figures 5A and 5B). The second hinge point is maintained by an interaction between loop $\beta5''/\beta6$ (at the guanine binding Asn306) and loop $\alpha9''/\alpha10$ (at the conserved Gly179) (green dot in Figures 5A and 5B). The swinging motion of the "bulk" of the synthetase domain (i.e., $\alpha12-\alpha15$) relative to the C3HB amounts to a 10° rotation about a pseudoaxis formed by these two main hinge points (Figure 5). However, $\alpha11$ cannot rotate in unison with the remaining bulk of the synthetase domain, since it is locked by its covalent and van der Waals association with $\alpha10$ of the C3HB. As a result, there is a collapse of cohesive motion within the synthetase domain, placing great strain on the linkage between $\alpha11$ and $\alpha12$ and driving a degeneration of ordered structure within this region in monomer 2 (hydrolase-ON/synthetase-OFF) (Figures 1 and 5).

The structural elements comprising $\alpha11$, loop $\alpha11/\alpha12$, and $\alpha12$ play an important functional role in Rel_{Seq} by forming a supportive framework for the underlying catalytic loop ($\alpha13/\beta4$) containing the essential Asp264 (Figure 4). In monomer 1 (hydrolase-OFF/synthetase-ON), loop $\alpha11/\alpha12$ is well-ordered and engages in a multitude of interactions with the catalytic loop, stabilizing the latter in a helical arrangement with Asp264 adopting the IN conformation situated alongside Glu323 for Mg^{2+}·ATP binding (Figure 4). However, in monomer 2 (hydrolase-ON/synthetase-OFF), the proximal termini of $\alpha11$ and $\alpha12$ are displaced due to the domain shifts and the intervening residues 211−216 (including the first two turns of $\alpha12$) become disordered (Figure 4). The disintegration of this supporting framework leads to an unfolding of the catalytic loop ($\alpha13/\beta4$) and the C terminus of $\alpha13$. Asp264 is thereby relocated to its inactive OUT conformation and residues 254–261 become disordered. Lys243, which we earlier implicated as a probable ATP-phosphate binding residue, undergoes a concomitant rearrangement away from the active site to interact with the backbone carbonyl of Leu265, thus stabilizing the OUT conformation of Asp264 (Figure 4). The dramatic rearrangement of residues 262−266 is visible as

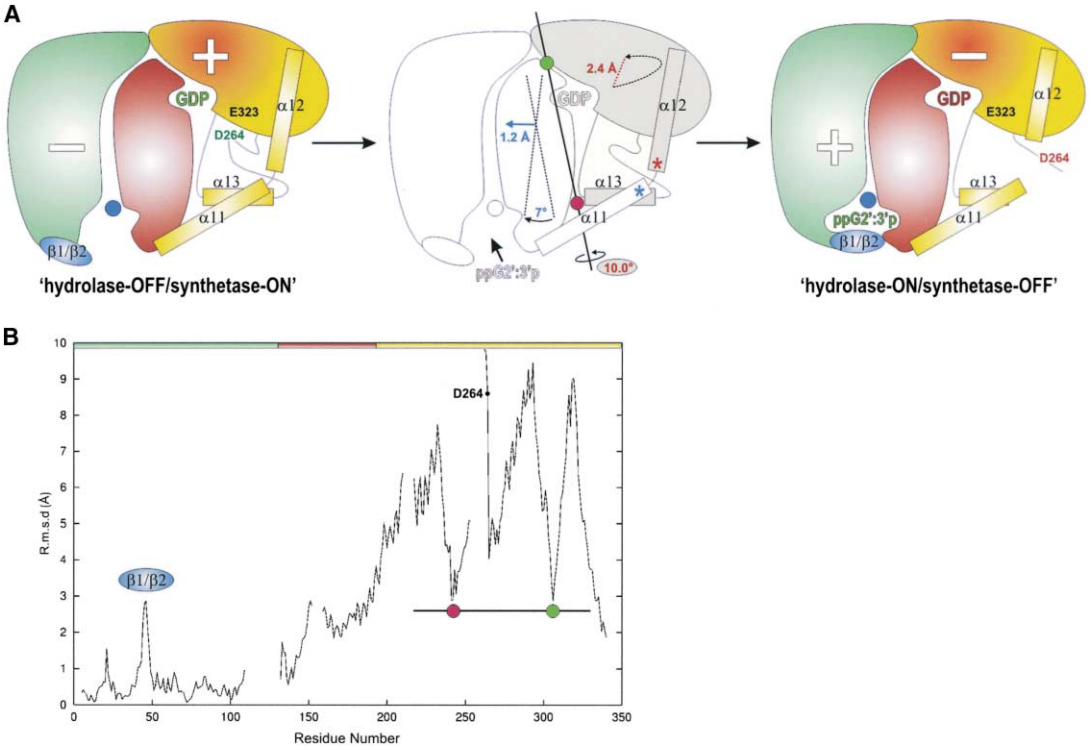

Figure 5. Signal Transmission from the Hydrolase Site to the Synthetase Site in Rel_{Seq}1–385

(A) Globular representations of Rel_{Seq}1–385 in the hydrolase-OFF/synthetase-ON (left) and hydrolase-ON/synthetase-OFF (right) conformations. Domain perspective and coloring is similar to that in Figure 1 (hydrolase, green/blue; C3HB, red; synthetase, yellow/orange). The IN and OUT conformations of Asp264 are labeled in green and red, respectively. The middle illustration depicts domain movements upon ligand binding to the hydrolase site. Translational and rotational components of the domain movements are labeled in blue (C3HB) and red (synthetase domain); corresponding blue and red asterisks indicate the α11/α12 linkage undergoing disruption due to the domain shifts. The synthetase-domain rotation axis and hinge points with the C3HB are represented by two colored circles and an intersecting line.

(B) Cα rmsd plot between the two conformations following least-squares superpositioning of residues 5−109 within the respective hydrolase domains. Breaks in the plot signify regions in either monomer where residues were disordered and could not be included in the calculation. A colored bar at the top of the plot delimits individual domains. Additional highlighted areas include the hydrolase β1/β2 hairpin displacement (blue), the rotational hinge points of the synthetase domain (magenta and green spheres corresponding to middle diagram of A), and the prominent displacement of the synthetase catalytic loop including Asp264 (labeled).

the most prominent peak in the atomic displacement profile given in Figure 5B and represents the pinnacle of the interdomain signal amplification cascade, which involves atomic shifts of more than ~10Å occurring at a distance of greater than 30 Å from the signal origin, the hydrolase active site.

Conclusions

Our structural investigations suggest a model for antagonistic regulation of (p)ppGpp synthesis and degradation based on combined principles of induced fit and intramolecular allosteric signaling between opposing active sites in the bifunctional Rel/Spo homologs. The structure suggests how the synthetase activity could be switched off as a consequence of the conformational changes triggered by nucleotide binding to the hydrolase domain. The reverse signaling pathway, from the synthetase site to the hydrolase site, seems equally likely and has preliminary support from the ability of an ATP-analog inhibitor of synthetase-mediated pyrophosphate transfer to inhibit the hydrolase. These same rearrangements are likely to play a role in furthering signals into the ribosome/tRNA binding C-terminal domain of Rel_{Seq}, which account for the inverse coupling of (p)ppGpp-synthesis and ribosome affinity in the case of RelA (Wendrich et al., 2002). The structural knowledge of the self-regulatory mechanisms proposed here for controlling the opposing catalytic activities of Rel_{Seq} can now be used to design specific inhibitors that interfere with either of the active sites and may have the potential of being developed into powerful antibacterial drugs.

Experimental Procedures

Protein Expression and Purification

Rel_{Seq}1–385 was produced from *E. coli* BL21 transformed with pENH385 (pET-21(+) (Novagen) carrying Rel_{Seq}1–385). Protein was purified as described before (Mechold et al., 2002) and stored in elution buffer at −20°C.

Crystallization

Thawed samples (10 mg protein/ml) were mixed with an equivolume of buffer solution containing 1 M NaCl, 4 mM GDP (Boehringer), 5 mM $MgCl_2$, and 5 mM MES [pH 6.0]. Well-diffracting crystals were obtained within 14 days in hanging drops by mixing 2 μl of this protein solution with an equivolume of reservoir solution containing 24%–36% PEG 8000, 0.6–1.0 M NaCl and 0.1 M Tris, pH 8.0–8.5, at room temperature. Crystals displayed space group C2, with unit

cell parameters a = 173.5 Å, b = 45.5 Å, c = 126.5 Å, and β = 109.8°. A V_m value of 2.55 Å^{3}Da^{-1} was calculated assuming two Rel_{Seq}1–385 molecules in the asymmetric unit, corresponding to a solvent content of 50% (Matthews, 1968).

Collection of Diffraction Data, MIR and MAD Analysis, Model Building, and Refinement

X-ray data to 2.1 Å resolution were collected at 100 K from a native crystal at EMBL beamline BW7B (DESY, Hamburg) with a MAR 345 image-plate detector (Table 1). All crystals were flash-cooled utilizing liquid paraffin oil as a cryoprotectant (Riboldi-Tunnicliffe and Hilgenfeld, 1999). Data were indexed, integrated, and scaled using the HKL suite (Otwinowski and Minor, 1997). Heavy-atom derivatization was achieved by introducing 1−5 mM of the respective heavy-atom compound into hanging drops containing the native crystals, followed by a soaking period of 1−14 days. Obtainment of suitable isomorphous derivative specimens was hampered by fluctuations of 3%–5% along the *b*-axis upon derivatization, and successful experimental phasing eventually required a combination of MAD and MIR techniques (Table 2). Initial mercury sites from a two-wavelength MAD dataset [ESRF beamline BM14 (Grenoble, France)] were extracted by the Patterson method and anomalous/dispersive difference Fourier analysis using CNS (Brünger et al., 1998), with subsequent MAD phasing conducted in SOLVE (Terwilliger and Berendzen, 1999). Additional phases were obtained with SOLVE from a MIR dataset consisting of the native data plus five heavy-atom derivatives (Table 2). Final experimental phases were derived by phase combination (Hendrickson and Lattman, 1970), yielding an overall figure of merit of 0.51 to 3.0 Å resolution. Substantial phase improvement was achieved after solvent flipping (Abrahams and Leslie, 1996), yielding an initial electron density map with a distinguishable protein-solvent barrier and several interpretable secondary structure elements. Iterative cycles of model building in O (Jones et al., 1991) were interspersed with rounds of phase combination, density modification, phase extension, and model refinement using experimental phase constraints in CNS. Despite the existence of two monomers in the asymmetric unit, the large global dissimilarities between them precluded the incorporation of non-crystallographic averaging and restraints during density modification and model refinement. High anisotropic diffraction was accounted for by an overall anisotropic temperature factor. Major improvements were achieved by application of TLS refinement [as implemented in REFMAC (CCP4, 1994; Winn et al., 2001)] in the final stages of model building and refinement. A total of three TLS groups per monomer were selected to model rigid anisotropic displacements within the respective (p)ppGppase, C3HB and (p)ppGpp-synthetase domains (including their associated ligands and water molecules), resulting in final R and R_{free} values of 0.239 and 0.273 for all data between 22.7−2.1 Å. Final refinement statistics are given in Table 1. Protein fold similarity searches were carried out using the Dali server (Holm and Sander, 1998). Molecular images were created with PyMOL (DeLano, 2002).

Mutational Analysis

Random transition mutations were obtained with mutagenic nucleotides (dPTP and oxo-dGTP, Amersham) by PCR of fragments encoding residues 1–72 or 73–224 (hydrolase mutants) or fragments 73–224 or 225–385 (synthetase mutants). Selection of hydrolase mutants in reconstituted fragment 1–224 after arabinose induction in a pBAD vector was by failure to relieve growth inhibition due to high basal levels of (p)ppGpp arising from a chromosomal SpoT203 allele. Selection for synthetase mutants within fragment 73–385 was by failure to achieve growth inhibition accompanying wild-type arabinose induction of synthetase expression. Mutant verification included controls for protein expression, growth tests, and sequencing. In some instances, mutants were reconstituted into the 1–385 fragment and activities assayed.

Effects of the Synthetase Inhibitor α,β-methylenyl ATP on pppGpp Hydrolysis

Rates of pppGpp degradation were measured as described for Figure 4 of Mechold et al. (2002) except that GTP (4 mM) was preincubated with 4 mM γ-[^{32}P]ATP to form 3′β-[^{32}P]pppGpp. Hydrolysis of pppGpp was measured as appearance of labeled pyrophosphate in the presence or absence of the synthetase inhibitor, α,β-methylenyl ATP (AMPCPP).

Acknowledgments

This work was, in part, supported by the DFG through grant Hi 611/1-3 to R.H. and H.M., who also thank the Fonds der Chemischen Industrie for continual support. This paper is dedicated to Wolfram Saenger on the occasion of his 65th birthday.

Received: September 26, 2003
Revised: January 13, 2004
Accepted: January 28, 2004
Published: April 1, 2004

References

Abrahams, J.P., and Leslie, A.G.W. (1996). Methods used in the structure determination of bovine mitochondrial F_1 ATPase. Acta Crystallogr. D *52*, 30–42.

Aravind, L., and Koonin, E.V. (1998). The HD domain defines a new superfamily of metal-dependent phosphohydrolases. Trends Biochem. Sci. *23*, 469–472.

Arndt, J.W., Gong, W., Zhong, X., Showalter, A.K., Liu, J., Dunlap, C.A., Lin, Z., Paxson, C., Tsai, M., and Chan, M.K. (2001). Insight into the catalytic mechanism of DNA polymerase: Structures of intermediate complexes. Biochemistry *40*, 5368–5375.

Avarbock, D., Avarbock, A., and Rubin, H. (2000). Differential regulation of opposing Rel_{Mtb} activities by the aminoacylation state of a tRNA-ribosome-mRNA-Rel_{Mtb} complex. Biochemistry *39*, 11640–11648.

Bourne, H.R., Sanders, D.A., and McCormick, F. (1990). The GTPase superfamily: a conserved switch for diverse cell functions. Nature *348*, 125–132.

Brünger, A.T., Adams, P.D., Clore, G.M., DeLano, W.L., Gros, P., Grosse-Kunstleve, R.W., Jiang, J., Kuzewski, J., Nilges, M., Pannu, N.S., et al. (1998). Crystallography and NMR System: a new software suite for macromolecular structure determination. Acta Crystallogr. D *54*, 905–921.

Cashel, M., Gentry, D.R., Hernandez, V.J., and Vinella, J. (1996). The Stringent Response. In *Escherichia coli* and *Salmonella*: cellular and molecular biology, C. Neidhardt, R. Curtiss III, J.L. Ingraham, E.C.C. Lin, K.B. Low, B. Magasanik, W.S. Reznikoff, M. Riley, M. Schaechter, and H.E. Umbarger, eds. (Washington, DC: ASM Press), pp. 1458–1496.

CCP4 (Collaborative Computational Project No. 4) (1994). The CCP4 suite: programs for protein crystallography. Acta Crystallogr. D *50*, 760–763.

Chatterji, D., and Ojha, A.K. (2001). Revisiting the stringent response, ppGpp and starvation signaling. Curr. Opin. Microbiol. *4*, 160–165.

Dahl, J.L., Krus, C.N., Boshoff, H.I.M., Doan, B., Foley, K., Avarbock, D., Kaplan, G., Mizrahi, V., Rubin, H., and Barry, C.E. (2003). The role of Rel_{Mtb}-mediated adaptation to stationary phase in long-term persistence of *Mycobacterium tuberculosis* in mice. Proc. Natl. Acad. Sci. USA *100*, 10026–10031.

DeLano, W.L. (2002). The PyMOL Molecular Graphics System. (San Carlos, CA: DeLano Scientific).

Givens, R.M., Lin, M.-H., Taylor, D.J., Mechold, U., Berry, J.O., and Hernandez, V.J. (2004). Inducible expression, enzymatic activity and origin of higher plant homologues of bacterial RelA/SpoT stress proteins in *nicotiana tabacum*. J. Biol. Chem. *279*, 7495–7504.

Goldbeter, A., and Koshland, D.E., Jr. (1987). Energy expenditure in the control of biochemical systems by covalent modification. J. Biol. Chem. *262*, 4460–4471.

Hammer, B.K., Tateda, E.S., and Swanson, M.S. (2002). A two-component regulator induces the transmission phenotype of stationary-phase *Legionella pneumophila*. Mol. Microbiol. *44*, 107–118.

Hendrickson, W.A., and Lattman, E.E. (1970). Representation of

phase probability distributions for simplified combination of independent phase information. Acta Crystallogr. B *26*, 136–143.

Holm, L., and Sander, C. (1995). DNA polymerase β belongs to an ancient nucleotidyltransferase superfamily. Trends Biochem. Sci. *20*, 345–347.

Holm, L., and Sander, C. (1998). Touring protein fold space with Dali/FSSP. Nucleic Acids Res. *26*, 316–319.

Hou, Z., Cashel, M., Fromm, H.J., and Honzatko, R.B. (1999). Effectors of the stringent response target the active site of *Escherichia coli* adenylosuccinate synthetase. J. Biol. Chem. *274*, 17505–17510.

Huai, Q., Wang, H., Sun, Y., Kim, H., Liu, Y., and Ke, H. (2003). Three-dimensional structures of PDE4D in complex with roliprams and implication on inhibitor selectivity. Structure *11*, 865–873.

Jones, T.A., Zou, J.Y., Cowan, S.W., and Kjeldgaard, M. (1991). Improved methods for building protein models in electron density maps and the location of errors in these models. Acta Crystallogr. A *47*, 110–119.

Kitamura, M., Kangawa, K., Matsuo, H., and Uyeda, K. (1988). Phosphorylation of myocardial fructose-6-phosphate, 2-kinase: fructose-2,6-bisphosphatase by cAMP-dependent protein kinase and protein kinase C. Activation by phosphorylation and amino acid sequences of the phosphorylation sites. J. Biol. Chem. *263*, 16796–16801.

Kuhar, I., van Putten, J.P., Zgur-Bertok, D., Gaastra, W., and Jordi, B.J. (2001). Codon-usage based regulation of colicin K synthesis by the stress alarmone ppGpp. Mol. Microbiol. *41*, 207–216.

Matthews, B.W. (1968). Solvent content of protein crystals. J. Mol. Biol. *33*, 491–497.

Mechold, U., and Malke, H. (1997). Characterization of the stringent and relaxed responses of *Streptococcus equisimilis*. J. Bacteriol. *179*, 2658–2667.

Mechold, U., Murphy, H., Brown, L., and Cashel, M. (2002). Intramolecular regulation of the opposing (p)ppGpp catalytic activities of Rel_{Seq}, the Rel/Spo enzyme from *Streptococcus equisimilis*. J. Bacteriol. *184*, 2878–2888.

Mildvan, A.S., Weber, D.J., and Abeygunawardana, C. (1999). Solution structure and mechanism of the MutT pyrophosphohydrolase. Adv. Enzymol. Relat. Areas Mol. Biol. *73*, 183–207.

Mittenhuber, G. (2001). Comparative genomics and evolution of genes encoding bacterial (p)ppGpp synthetases/hydrolases (the Rel, RelA and SpoT proteins). J. Mol. Microbiol. Biotechnol. *3*, 585–600.

Otwinowski, Z., and Minor, W. (1997). Processing of X-ray diffraction data collected in oscillation mode. Methods Enzymol. *276*, 307–326.

Pao, C.C., and Dyess, B.T. (1981). Effect of unusual guanosine nucleotides on the activities of some *Escherichia coli* cellular enzymes. Biochim. Biophys. Acta *677*, 358–362.

Pao, C.C., Dennis, P.P., and Gallant, J.A. (1980). Regulation of ribosomal and transfer RNA synthesis by guanosine 5′-diphosphate-3′-monophosphate. J. Biol. Chem. *255*, 1830–1833.

Riboldi-Tunnicliffe, A., and Hilgenfeld, R. (1999). Cryocrystallography with oil—an old idea revived. J. Appl. Crystallogr. *32*, 1003–1005.

Sawaya, M.R., Prasad, R., Wilson, S.H., Kraut, J., and Pelletier, H. (1997). Crystal structures of human DNA polymerase β complexed with gapped and nicked DNA: evidence for an induced fit mechanism. Biochemistry *36*, 11205–11215.

Steiner, K., and Malke, H. (2000). Life in protein-rich environments: the *relA*-independent response of *Streptococcus pyogenes* to amino acid starvation. Mol. Microbiol. *38*, 1004–1016.

Sun, J., Hesketh, A., and Bibb, M. (2001). Functional analysis of relA and rshA, two relA/spoT homologues of *Streptomyces coelicolor* A3(2). J. Bacteriol. *183*, 3488–3498.

Terwilliger, T.C., and Berendzen, J. (1999). Automated MAD and MIR structure solution. Acta Crystallogr. D *55*, 849–861.

van Delden, C., Comte, R., and Bally, A.M. (2001). Stringent response activates quorum sensing and modulates cell density-dependent gene expression in *Pseudomonas aeruginosa*. J. Bacteriol. *183*, 5376–5384.

van der Biezen, E.A., Sun, J., Coleman, M.J., Bibb, M.J., and Jones, J.D.G. (2000). *Arabidopsis* RelA/SpoT homologs implicate (p)ppGpp in plant signaling. Proc. Natl. Acad. Sci. USA *97*, 3747–3752.

Walker, J.E., Saraste, M., Runswick, M.J., and Gay, N.J. (1982). Distantly related sequence in the α- and β-subunits of ATP synthetase, myosin, kinases, and other ATP-requiring enzymes and a common nucleotide binding fold. EMBO J. *1*, 945–951.

Weiss, M.S., and Hilgenfeld, R. (1997). On the use of the merging R factor as a quality indicator for X-ray data. J. Appl. Crystallogr. *30*, 203–205.

Wendrich, T.M., Beckering, C.L., and Marahiel, M.A. (2000). Characterization of the *relA/spoT* gene from *Bacillus stearothermophilus*. FEMS Microbiol. Lett. *190*, 195–201.

Wendrich, T.M., Blaha, G., Wilson, D.N., Marahiel, M.A., and Nierhaus, K.H. (2002). Dissection of the mechanism for the stringent factor RelA. Mol. Cell *10*, 779–788.

Winn, M.D., Isupov, M.N., and Murshudov, G.N. (2001). Use of TLS parameters to model anisotropic displacements in macromolecular refinement. Acta Crystallogr. D *57*, 122–133.

Xu, R.X., Hassell, A.M., Vanderwall, D., Lambert, M.H., Holmes, W.D., Luther, M.A., Rocque, W.J., Milburn, M.V., Zhao, Y., Ke, H., and Nolte, R.T. (2000). Atomic structure of PDE4: insights into phosphodiesterase mechanism and specificity. Science *288*, 1822–1825.

Accession Numbers

Atomic coordinates of the structure described here as well as the experimental diffraction amplitudes have been deposited in the Protein Data Bank with accession number 1VJ7.